Formation of stable HCl^+ following resonant Auger decay in CH_3Cl

E. Kokkonen,[1,*] M. Vapa,[1,2] K. Bučar,[3] K. Jänkälä,[1] W. Cao,[1] M. Žitnik,[3,4] and M. Huttula[1]

[1]*Nano and Molecular Systems Research Unit, University of Oulu, P.O. Box 3000, FIN-90014 Oulu, Finland*

[2]*Department of Theoretical Chemistry and Biology, School of Biotechnology, KTH Royal Institute of Technology, SE-10691 Stockholm, Sweden*

[3]*Jožef Stefan Institute, Jamova 39, SI-1000 Ljubljana, Slovenia*

[4]*Faculty of Mathematics and Physics, University of Ljubljana, Jadranska 19, SI-1000 Ljubljana, Slovenia*

(Received 28 June 2016; published 12 September 2016)

Photoinduced reformation of chemical bonds is investigated in the CH_3Cl molecule experimentally and computationally. The observation of stable HCl^+ fragment formation after resonant Cl $2p$ photoexcitation is confirmed by an electron-ion coincidence experiment, and its possible creation mechanism is reported. We attribute the formation of HCl^+ to specific final states populated by the resonant Auger decay. Quantum chemical computations support this attribution and suggest that in at least one of those states the system is placed on a potential energy surface which favors creation of HCl^+ by moving one hydrogen atom to a closer proximity of the chlorine atom. This work demonstrates the effect of targeted core-shell excitation on the chemical bond breaking and reformation process, often called photoinduced chemistry.

DOI: 10.1103/PhysRevA.94.033409

I. INTRODUCTION

Chemical bonds are normally formed during chemical reactions when molecular valence electrons are recoupled after breaking the original bonds. In case of larger molecules such as DNA, it has been found that it is possible to selectively prepare individual bonds by placing functional groups of reactant molecules accordingly in the macromolecular structure [1]. Reactant valence bond breaking can be realized through various means. Besides direct photodissociation via ionization of molecular valence orbitals, bond breaking may also be induced by the resonant Auger (RA) decay process where the electron is prompted to an unoccupied molecular orbital and the core-hole is filled via electron pair interaction leading finally to an ejection of RA electron from the valence orbital. For small molecules, the promotion of an electron to the antibonding σ^* orbital already triggers a dissociation which may occur on a timescale comparable to the RA decay [2–4], making the rebinding of formed fragments very unlikely [5–7].

To probe molecular dissociation and recombination dynamics subsequent to the Auger decay in small systems, the chloromethane (CH_3Cl) molecule was selected as a target due to its importance in a multitude of industrial applications and (as part of organochlorides) in living organisms [8]. Dissociation of chloromethane subsequent to a core-hole creation has been extensively studied in carbon K shell excitations [9–12] as well as in the vicinity of chlorine L shell [13,14]. The appearance of a HCl^+ fragment subsequent to the excitation of the Cl $2p$ electron to the unoccupied σ^* orbital has been reported before [13,14], but the exact formation route of HCl^+ has not been fully explored. In Ref. [14], the creation of HCl^+ was explained via a fragmentation of CH_3Cl into outgoing Cl^+ and vibrationally excited CH_3 leading to a situation where it is likely that a hydrogen atom is left trapped to form rovibrationally excited HCl^+.

In the current work we study the movement of the hydrogen atoms in the CH_3Cl molecule using extensive Auger-electron fragment-ion coincidence measurements as well as quantum chemical calculations for qualitative analysis. We specify a possible pathway for the formation of stable HCl^+. The electron-ion coincidence experiments were conducted in such a way that also the photon energy was changed in small steps, giving us another dimension from which to observe the dissociation phenomena in the CH_3Cl molecule.

II. EXPERIMENTAL DETAILS

The experiments were conducted at the I411 beamline [15,16] of the MAX II storage ring in the MAX IV Laboratory, Lund, Sweden. The electron-ion coincidence spectra were obtained using a modified Scienta SES-200 type electron spectrometer with a resistive anode detector for fast electron detection. The signal from the electron spectrometer serves as the starting point for the measurement of the masses of the ions using a Wiley-McLaren type [17] time-of-flight mass spectrometer (TOFMS) (similar coincidence setups have been described previously, e.g., in [18–21] and references therein). For the coincidence measurements the electron spectrometer was operated with a constant pass mode with pass energies of 100 and 200 eV and with curved entrance slit width of 0.8 mm, which provide approximate analyzer line broadenings of 0.2 and 0.4 eV, respectively. All experiments were conducted with the analyzer at the so-called "magic" angle of 54.7° with respect to the electric field vector of the linearly polarized light. At this geometry the photoemission angular distribution parameters do not affect the observed intensity, being only proportional to the angle integrated photoionization cross section [22]. The photon energy scale was calibrated by independent total ion yield (TIY) measurements.

Gaseous CH_3Cl (purity >99.5%) was fed into the vacuum chamber via a thin needle, which enabled a higher sample pressure in the interaction region. The total pressure in the chamber during measurements was in the 10^{-6} mbar range.

*esko.kokkonen@oulu.fi

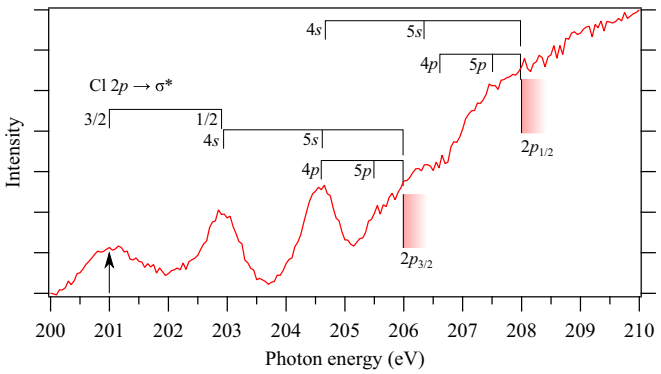

FIG. 1. TIY spectrum of the CH_3Cl molecule across the Cl $2p$ excitation thresholds. The arrow indicates the Cl $2p_{3/2} \rightarrow \sigma^*$ resonance, which was the excitation energy used for the spectrum in Fig. 4. The excitations to the valence and Rydberg orbitals and the $2p$ ionization thresholds are drawn according to Ref. [23].

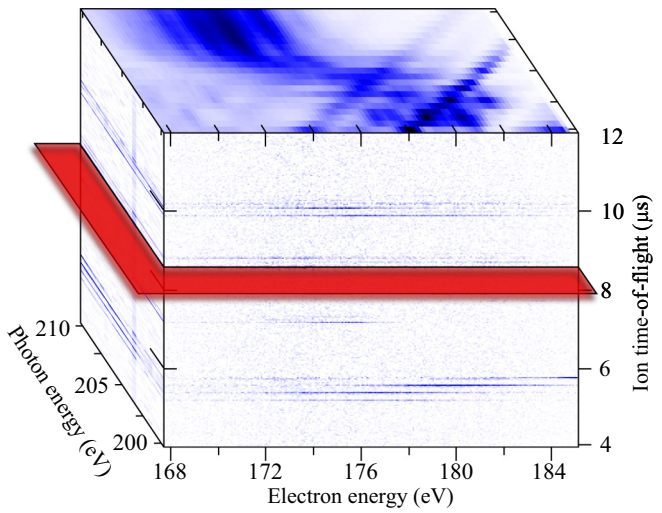

FIG. 2. The entire set of three-dimensional coincidence data displayed on a cube. The faces are chosen to show projections of the entire data in their respective directions, in order to illustrate the complexity of the data. A slice that forms one of the 2D maps in Fig. 3 is indicated by the plane intersecting the cube.

III. RESULTS AND DISCUSSION

A. Electron-ion coincidence results

The absorption spectrum of CH_3Cl exhibits several pronounced resonances prior to the $2p$ ionization threshold as indicated in the TIY spectrum in Fig. 1.

In this work the coincidence experiments were tuned to the Cl $2p$ resonances and a few eV above the ionization threshold. Conventional energy resolved electron-ion coincidence experiments focus on the production of specific fragment ions, which is linked to the emitted electrons due to the nonradiative decay of the initial photoexcited state of the molecule, often measured at fixed photon energy. Here, however, we have extended the conventional coincidence experiment by performing a "scanned" coincidence measurement where also the photon energy was changed in small steps across the chlorine $2p$ region while keeping the electron energy window fixed. The method resembles constant final state (CFS) spectroscopy, where the photon energy is scanned over the desired region and electron energies from a fixed kinetic energy range are collected. Here, in addition to collecting electrons from specific final states that are present in the energy window, we also get information of the masses of the ions that were formed subsequent to creation of the selected final states. Since in our case the kinetic energy range of the electrons was kept fixed, the final states that are photon energy dependent create diagonal lines across the window (direct photoionization and RA decay), and final states which are approximately photon independent stay at the same kinetic energies (normal Auger decay), as can be seen on the top of the cube in Fig. 2. We therefore call this method coincident constant final state (CO-CFS) spectroscopy.

In the current experiment, we have scanned the photon energy in the region of 200–210 eV with 0.5 eV steps while keeping the electron kinetic energy window fixed at approximately 168–184 eV. We therefore get a three-dimensional data set, with perpendicular axes for photon and electron energies and ion time-of-flight (or mass). These data are presented, for visualization only, in Fig. 2 as a cube with the colors of the pixels indicating intensity. CO-CFS data are very useful when observing and visualizing the complete energy and mass resolved excitation decay and fragmentation events. To display the needed quantitative information, the dataset is sliced in the desired dimension. A possible way of slicing is, for example, to pick a specific mass range and plot the amount of coincident ions in a two-dimensional (2D) map as a function of photon and electron energies, denoting intensity of the formed ion with color. These 2D coincident ion yield (2D-CIY) maps have been formed in Fig. 3 for the ions Cl^+, HCl^+, CH_3^+, CH_2^+, and the CH_nCl^+ ($n = 3$–0) species. An exception is Fig. 3(a) where only the noncoincident electrons are depicted, which means that panel (a) now gives a more conventional CFS map of the region.

From Fig. 3(a), diagonal lines are clearly seen, where the most intense line starting at kinetic energy of approximately 178 eV (~22 eV binding energy) corresponds to a direct photoionization of the inner valence molecular orbital $2a_1$ (in C_{3v} symmetry) [24–27]. To better guide the eye, a dotted black diagonal line has also been drawn in all of the panels depicting the binding energy of the $2a_1$ orbital. Dissociation subsequent to ionization from this orbital is clearly leading to a release of a CH_2^+ fragment, since its intensity stays rather constant across the measured region. The other dotted black diagonal line starting at kinetic energy of 174 eV represents ionization from the $1a_1$ molecular orbital, which has a binding energy of about 26 eV [26,27]. Due to the low intensity of the photoelectrons from this orbital, we cannot identify with absolute certainty the full fragmentation pattern, but at least C^+, CH^+, and some CH_nCl^+ species are found in coincidence with the photoelectrons emitted from this valence orbital. In the lower right corner of the window there is also some contribution coming from ionizations of the $1e$ orbital, which then moves out of the window as photon energy is increased. Ionization of the $1e$ orbital appears to dissociate the molecule by releasing a CH_3^+ fragment [28].

Beyond the valence states and other ionized states reached by RA decay, above the $2p$ ionization threshold (at approximately $h\nu = 206$ eV), electrons from the normal

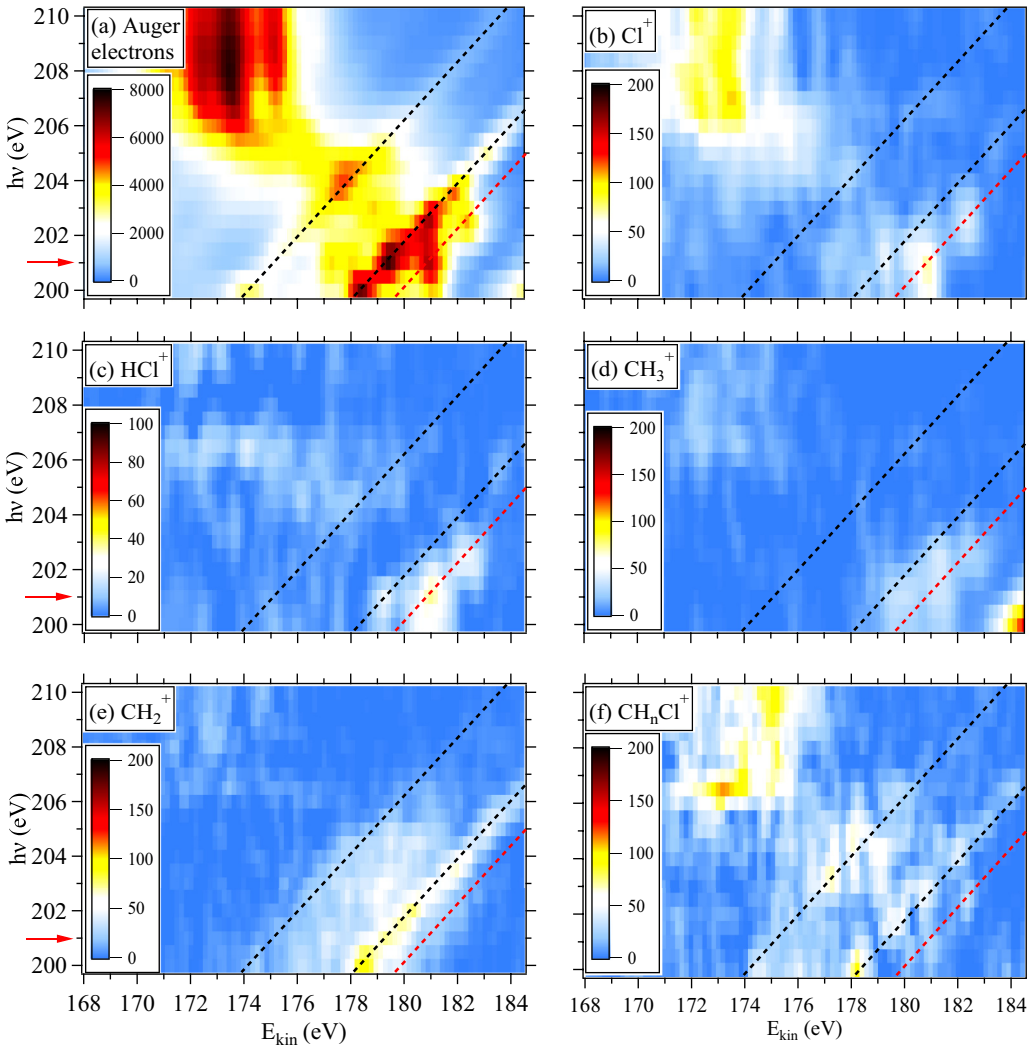

FIG. 3. 2D-CIY maps as a function photon and electron energies for (a) Auger electrons, (b) Cl^+ fragment, (c) HCl^+ fragment, (d) CH_3^+ fragment, (e) CH_2^+ fragment, and (f) CH_nCl^+ fragments ($n = 3$–0). Black dashed diagonal lines represent the $1a_1$ and $2a_1$ valence molecular orbital signals moving as a function of photon energy, and the red diagonal signal represents the final states of the RA decay and possible shake-up processes (see text for details). The red arrows indicate the position of the σ^* resonance which was photoexcited to obtain data presented in Fig. 4.

Auger process dominate the spectrum at kinetic energies of 168–176 eV.

From Fig. 3(c) it is clear that the production of HCl^+ is related to the final states populated at $h\nu = 201$ eV and most intensely in coincidence with the states with electron energy of approximately 181 eV (20 eV binding). For HCl^+, we can conclude that its formation requires the population of unoccupied molecular orbitals. From the current experiment it is obvious that the final state is mostly reached through the RA decay, but there is also a small probability of a direct valence photoionization accompanied by a shake-up process. The final state that is reached in these situations is depicted by the red diagonal line in the panels of Fig. 3. It is clear, however, that the cross section for valence photoionization and especially photoionization combined with a shake-up process is very low at the selected photon energies (~201 eV).

A likely scheme for the HCl^+ creation pathway is through the initial promotion of an Cl $2p$ electron to the unoccupied σ^* orbital, following with the RA decay. It is also worth noting that, while there is a nonzero probability that the HCl^+ could originate due to a fortuitous recombination between the residual hydrogen and chlorine leftover from other dissociations, our observations clearly exclude this possibility.

To get a more detailed picture of the final states that are in coincidence with HCl^+ fragment, we have further sliced the CO-CFS data in Fig. 2 to present CIYs at the resonant photon energy of 201 eV to match the σ^* resonance. The electron window was set at approximately 176–183 eV (25–18 eV binding energy) to see the Cl $2p$ RA final states. In Fig. 4 we have depicted the electron spectrum at the top and the Cl^+, HCl^+, CH_3^+ and CH_2^+ CIY spectra below.

The noncoincidence electron spectrum at the top of Fig. 4 shows that there are roughly two regimes regarding Auger decay of the $2p$ hole in the molecule, depending on whether it occurs fast or slow with respect to the dissociation dynamics. The three labeled peaks originate from the ultrafast dissociation of CH_3Cl, where the Auger decay is slower than the dissociation. In this case, the Auger electron

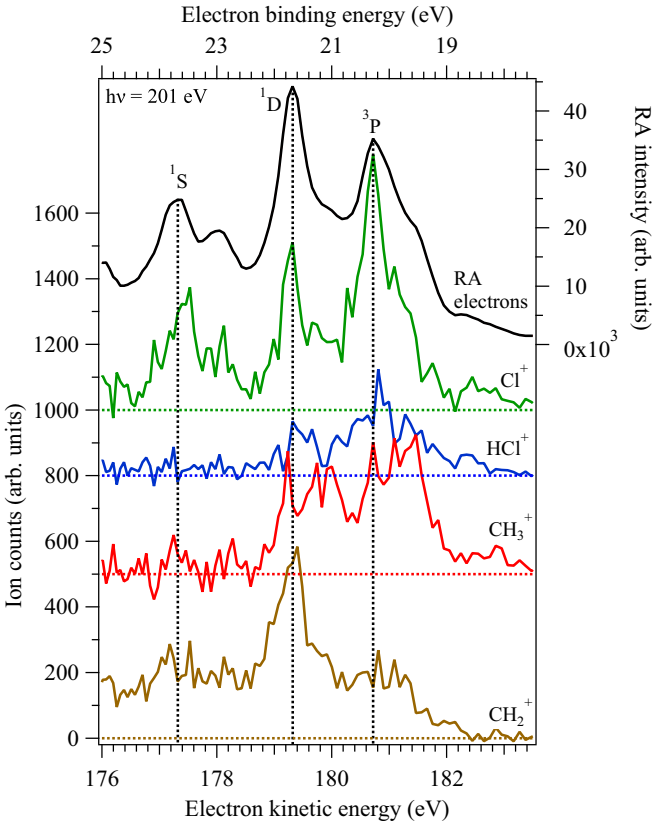

FIG. 4. CIY spectra of the Cl^+, HCl^+, CH_3^+, and CH_2^+ fragments and the RA electron spectrum (top) on the Cl $2p \rightarrow \sigma^*$ resonance. The horizontal dashed lines represent the background levels for the CIYs and the vertical lines are drawn to guide the eye along the positions of atomic Cl ^1S, ^1D, and ^3P states. Assignments according to Ref. [29].

is ejected from the chlorine atom, and therefore the peaks correspond well with the atomic chlorine signal according to the energies of the Auger final states ^1S, ^1D, or ^3P, which are emphasized with the dashed lines in Fig. 4 [14]. Superimposed with these peaks is the broader Auger background signal originating from the transient molecular complex. In these Auger final states, the RA decay is faster than dissociation, and the signal originates from the still intact molecule. The origin of the HCl^+ fragment is of interest in this study, and according to the results, it coincides with the broader molecular Auger signal at approximately 181 eV (kinetic) and 20 eV (binding).

The high amount of CH_2^+ cation observed in Fig. 4 is due to the direct photodissociation of one of the valence orbitals which causes CH_2^+ fragment to be released, as discussed above in the broader context of the entire CO-CFS data.

CH_3^+ fragment is seen to coincide with the same Auger final states as HCl^+. This would indicate that both cations originate from the same process (i.e., from the breaking of the C—Cl bond), with the notable exception that the case that produces CH_3^+ obviously involves no significant hydrogen movement towards the chlorine atom, which remains neutral.

B. Computational results

To illustrate the RA decay mechanism leading to HCl^+ formation, we employed quantum chemical computations to predict the Auger electron energies and the dynamics of the photoexcited system. The two-step Auger emission process in the resonance states is

$$M + h\nu \rightarrow M^* \rightarrow M^{*+} + e^-_{\text{Auger}}, \tag{1}$$

where M is the original CH_3Cl molecule, M^* the first exited state, and M^{*+} the final state after Auger decay. To identify the possible final states M^{*+} that follow from the Auger process we can use the equation

$$E(M) + h\nu = E_{\text{kin}}(e^-_{\text{Auger}}) + E(M^{*+}). \tag{2}$$

Using the CH_3Cl molecule ground state energy $E(M)$ and the final state energies $E(M^{*+})$, it is possible to associate the different Auger kinetic energies with their respective final states. Here it is also assumed that any kinetic energy gained by the ion is contained within $E(M^{*+})$. The ground state energy was calculated by the multiconfiguration self-consistent-field (MCSCF) method. Using the ground state wave functions as the starting orbitals, an MCSCF energy calculation was performed for excited final state. Six occupied valence orbitals and the σ^* orbital formed the active space with one electron missing from the system. All computations were performed using the DALTON quantum chemistry code package [30] with Aug-cc-pVTZ basis sets for all atoms.

Using Eq. (2), the energies of the Auger electrons were calculated, where $E(M^{*+})$ now corresponds to a state where the σ^* orbital is singly occupied and there are two holes in the inner valence. The situations where the holes are in the outer valence give energies much lower than the experimental values. Four final states were found where the RA electron energy is 181.56, 181.42, 181.40, and 181.03 eV, which correspond well to the energies in the experimental spectrum where the HCl^+ fragment production is seen.

To further study the dissociation mechanism, the internal dynamics in the singly occupied σ^* final state were modeled. This was performed via a restricted active space self-consistent field (RASSCF) geometry optimization. The four configurations from the energy calculations with an electron on the σ^* orbital and two holes in the inner valence were selected. Each of these four excited states was then subjected to a geometry optimization routine starting from the ground state atomic positions. The routine calculates the internal forces of the system and moves the atoms along the gradient of the potential in a sequence of steps until all the driving forces are sufficiently small. Obviously, this is not equivalent to a time-dependent solution of the Schrödinger equation for a dissociating molecule, but still the optimization is able to trace out ways along which atoms move in order to adjust to the change of the potential triggered by population of the selected final electronic state. It has been shown [10,11] that the electron transfer from an inner orbital to σ^* initiates molecular dissociation along the C—Cl coordinate. However, as Cl $2p$ core-hole decay is very fast (3–7 fs [3,31]) the C—Cl distance change before RA decay is small (0.1–0.2 Å). As we are dealing with nuclear dynamics subsequent to the molecular Auger decay, our optimization procedure therefore fixes the C—Cl bond length to the ground state value and focuses on much faster movements of the hydrogen atoms in the system. Bond length restriction approximation is a common way of

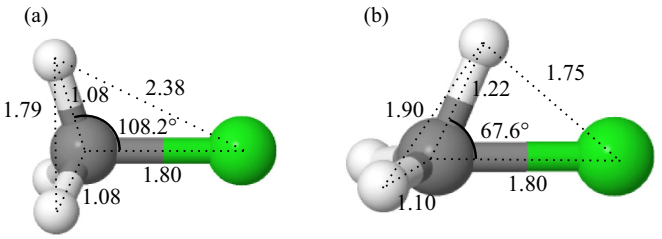

FIG. 5. (a) Initial ground state geometry of the CH_3Cl molecule. (b) Geometry of the molecule after eight iterations of the optimization cycle in the selected configuration. The molecule displays rotation of the methyl group towards the Cl atom. All bond lengths are in Å.

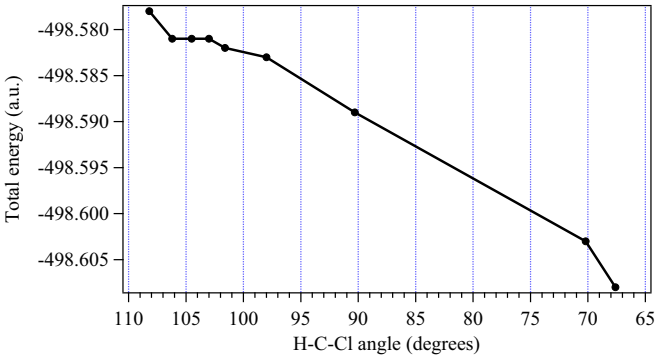

FIG. 6. Total energy of the molecule as a function of the H—C—Cl angle.

reducing the degrees of freedom in order to aid the electronic structure and nuclear dynamics calculations [32].

In three of the four calculations differing in final RA state, the optimization routine gives no indication of behavior which would create HCl^+. However, in one case, the methyl group rotates in such a way that one of the hydrogen atoms ends up closer to the chlorine atom and the other two hydrogen atoms lie roughly in the same plane with the carbon and chlorine atoms as seen in Fig. 5. The computational kinetic energy for this state agrees well with the experimental finding which is that the HCl^+ formation happens most intensely at kinetic energies of approximately 181 eV. Tabulating the total energies along the optimization steps shows that one hydrogen has a path of decreasing energy along which the HCl^+ is formed, at least in the initial excited state of the molecule. Figure 5(b) shows the geometry of the molecule after eight iterations of the geometry optimization routine for the selected final state. This can be compared to Fig. 5(a) showing the initial ground state geometry of the CH_3Cl molecule. Figure 6 shows the total energy of the molecule during the first eight iterations of the geometry optimization as a function of the H—C—Cl angle.

However, after initially optimizing one of the hydrogens towards the chlorine atom for several steps, the routine suddenly changes direction and begins distancing the hydrogen atom from the parent molecule, perpendicular to the C–Cl axis. We attribute this sudden change in the potential gradient to a crossing of the potential energy surfaces of two different states at the particular coordinates. As the optimization only converges to the lowest root (with the specific symmetry and multiplicity), it cannot follow the original state beyond that point. A possible solution would be to restart the calculation at the divergence point and follow the second lowest state instead of the lowest one, but the large computational requirements put that outside the scope of this study. Regardless, the initial optimization steps clearly indicate that the internal forces of the excited molecule provide a potential pathway for the translation of a hydrogen atom to closer proximity with the chlorine atom.

IV. CONCLUSION

In summary, we have performed a photon energy scanned electron-ion coincidence experiment, which we call coincident constant final state spectroscopy. The CO-CFS results verify the appearance of stable HCl^+ in coincidence with the specific final state of the resonant Auger decay at the $2p \rightarrow \sigma^*$ resonance. This indicates that the formation of HCl^+ from the initially neutral CH_3Cl molecule requires the population of orbitals of the strongly antibonding σ type relaxed by the fast resonant Auger decay into the specific final states at ~20 eV binding energy.

To support the experimental findings, we performed qualitative theoretical simulations on the dynamics of the hydrogen movement, and found that in the specific Auger final state, the methyl group does indeed gain rotational momentum, which would bring one of the hydrogens closer to the chlorine atom. More detailed calculations are, however, required to fully realize the multidimensional potential energy surfaces in the system in the ionized and excited states.

ACKNOWLEDGMENTS

Staff of the MAX IV Laboratory are acknowledged for assistance in I411 beamline operation. The work is financially supported by an Oulu University Strategic Grant, the P1-0112 research program of the Slovenian Research Agency, the Magnus Ehrnrooth Foundation, the Vilho, Yrjö and Kalle Väisälä Foundation, the North Ostrobothnia Regional fund of the Finnish Cultural Foundation, and the Research Council for Natural Sciences and Engineering of the Academy of Finland. The research leading to these results has also received funding from the European Community's Seventh Framework Programme (FP7/2007-2013) CALIPSO under Grant Agreement No. 312284.

[1] N. Voigt, T. Tørring, A. Rotaru, M. Jacobsen, J. Ravnsbæk, R. Subramani, W. Mamdouh, J. Kjems, A. Mokhir, F. Besenbacher, and K. Gothelf, Nat. Nanotechnol. **5**, 200 (2010).

[2] P. Morin and I. Nenner, Phys. Rev. Lett. **56**, 1913 (1986).

[3] H. Aksela, S. Aksela, M. Ala-Korpela, O.-P. Sairanen, M. Hotokka, G. M. Bancroft, K. H. Tan, and J. Tulkki, Phys. Rev. A **41**, 6000 (1990).

[4] O. Travnikova, T. Marchenko, G. Goldsztejn, K. Jänkälä, N. Sisourat, S. Carniato, R. Guillemin, L. Journel, D. Céolin, R. Püttner *et al.*, Phys. Rev. Lett. **116**, 213001 (2016).
[5] K. Ueda, M. Simon, C. Miron, N. Leclercq, R. Guillemin, P. Morin, and S. Tanaka, Phys. Rev. Lett. **83**, 3800 (1999).
[6] O. Travnikova, V. Kimberg, R. Flammini, X.-J. Liu, M. Patanen, C. Nicolas, S. Svensson, and C. Miron, J. Phys. Chem. Lett. **4**, 2361 (2013).
[7] M. N. Piancastelli, R. Guillemin, M. Simon, H. Iwayama, and E. Shigemasa, J. Chem. Phys. **138**, 234305 (2013).
[8] G. W. Gribble, Pure Appl. Chem. **68**, 1699 (1996).
[9] L. El Khoury, L. Journel, R. Guillemin, S. Carniato, W. C. Stolte, T. Marin, D. W. Lindle, and M. Simon, J. Chem. Phys. **136**, 024319 (2012).
[10] R. Bohinc, M. Žitnik, K. Bučar, M. Kavčič, L. Journel, R. Guillemin, T. Marchenko, M. Simon, and W. Cao, J. Chem. Phys. **139**, 134302 (2013).
[11] R. Bohinc, M. Žitnik, K. Bučar, and M. Kavčič, J. Chem. Phys. **140**, 164304 (2014).
[12] R. Bohinc, M. Žitnik, K. Bučar, M. Kavčič, S. Carniato, L. Journel, R. Guillemin, T. Marchenko, E. Kawerk, M. Simon *et al.*, J. Chem. Phys. **144**, 134309 (2016).
[13] D. Céolin, M. N. Piancastelli, R. Guillemin, W. C. Stolte, S.-W. Yu, O. Hemmers, and D. W. Lindle, J. Chem. Phys. **126**, 084309 (2007).
[14] C. Miron, P. Morin, D. Céolin, L. Journel, and M. Simon, J. Chem. Phys. **128**, 154314 (2008).
[15] M. Bässler, J.-O. Forsell, O. Björneholm, R. Feifel, M. Jurvansuu, S. Aksela, S. Sundin, S. Sorensen, R. Nyholm, A. Ausmees, and S. Svensson, J. Electron Spectrosc. Relat. Phenom. **101–103**, 953 (1999).
[16] M. Bässler, A. Ausmees, M. Jurvansuu, R. Feifel, J.-O. Forsell, P. de Tarso Fonseca, A. Kivimäki, S. Sundin, S. Sorensen, R. Nyholm, O. Björneholm, S. Aksela, and S. Svensson, Nucl. Instrum. Meth. A **469**, 382 (2001).
[17] W. C. Wiley and I. H. McLaren, Rev. Sci. Instrum. **26**, 1150 (1955).
[18] E. Kukk, R. Sankari, M. Huttula, A. Sankari, H. Aksela, and S. Aksela, J. Electron Spectrosc. Relat. Phenom. **155**, 141 (2007).
[19] J. A. Kettunen, S. Urpelainen, S. Heinäsmäki, and M. Huttula, Phys. Rev. A **86**, 023201 (2012).
[20] E. Kokkonen, T. Löytynoja, K. Jänkälä, J. A. Kettunen, S. Heinäsmäki, A. Karpenko, and M. Huttula, J. Chem. Phys. **140**, 184304 (2014).
[21] E. Kokkonen, T. Löytynoja, L. Hautala, K. Jänkälä, and M. Huttula, J. Chem. Phys. **143**, 074307 (2015).
[22] V. Jacobs, J. Phys. B: At. Mol. Phys. **5**, 2257 (1972).
[23] R. Thissen, M. Simon, and M.-J. Hubin-Franskin, J. Chem. Phys. **101**, 7548 (1994).
[24] W. von Niessen, L. Åsbrink, and G. Bieri, J. Electron Spectrosc. Relat. Phenom. **26**, 173 (1982).
[25] I. Novak, J. Benson, and A. Potts, J. Electron Spectrosc. Relat. Phenom. **41**, 225 (1986).
[26] T. N. Olney, W. F. Chan, G. Cooper, C. Brion, and K. Tan, J. Electron Spectrosc. Relat. Phenom. **66**, 83 (1993).
[27] D. Holland, I. Powis, G. Öhrwall, L. Karlsson, and W. von Niessen, Chem. Phys. **326**, 535 (2006).
[28] R. Locht, B. Leyh, A. Hoxha, D. Dehareng, K. Hottmann, H. Jochims, and H. Baumgärtel, Chem. Phys. **272**, 293 (2001).
[29] O. Björneholm, S. Sundin, S. Svensson, R. R. T. Marinho, A. Naves de Brito, F. Gel'mukhanov, and H. Ågren, Phys. Rev. Lett. **79**, 3150 (1997).
[30] K. Aidas, C. Angeli, K. L. Bak, V. Bakken, R. Bast, L. Boman, O. Christiansen, R. Cimiraglia, S. Coriani, P. Dahle *et al.*, WIREs Comput. Mol. Sci. **4**, 269 (2015).
[31] P. Morin and C. Miron, J. Electron Spectrosc. Relat. Phenom. **185**, 259 (2012).
[32] E. Kawerk, S. Carniato, L. Journel, T. Marchenko, M. N. Piancastelli, M. Žitnik, K. Bučar, M. Kavčič, D. Céolin, A. Khoury *et al.*, J. Chem. Phys. **141**, 144301 (2014).